



## Supporting Online Material for

### **Dynamic Ca<sup>2+</sup>-Dependent Stimulation of Vesicle Fusion by Membrane-Anchored Synaptotagmin 1**

Han-Ki Lee, Yoosoo Yang, Zengliu Su, Changbong Hyeon, Tae-Sun Lee,  
Hong-Won Lee, Dae-Hyuk Kweon, Yeon-Kyun Shin, Tae-Young Yoon

\*To whom correspondence should be addressed.

E-mail: colishin@iastate.edu (Y.-K.S.); tyyoon@kaist.ac.kr (T.-Y.Y.)

Published 7 May 2010, *Science* **328**, 760 (2010)

DOI: 10.1126/science.1187722

#### **This PDF file includes:**

Materials and Methods  
SOM Text  
Figs. S1 to S9  
Table S1  
References

**Other Supporting Online Material for this manuscript includes the following:**  
(available at [www.sciencemag.org/cgi/content/full/328/5979/760/DC1](http://www.sciencemag.org/cgi/content/full/328/5979/760/DC1))

Movie S1

# **Dynamic Ca<sup>2+</sup>-Dependent Stimulation of Vesicle Fusion by Membrane-Anchored Synaptotagmin 1**

Han-Ki Lee, Yoosoo Yang, Zengliu Su, Changbong Hyeon, Tae-Sun Lee, Hong-Won Lee, Dae-Hyuk Kweon, Yeon-Kyun Shin and Tae-Young Yoon

## **SUPPORTING ONLINE MATERIALS**

This supplement contains:

Materials and Methods

Supporting Online Material Text

fig. S1 to S9

Table S1

Supporting Movie Caption

References

## Materials and Methods

**Protein expression and purification** Recombinant neuronal SNARE proteins from rat: syntaxin 1A (Syn1A; amino acids 1- 288), SNAP-25 (amino acids 1-206), synaptobrevin 2 (Syb2; amino acids 1-116) and soluble C2AB (amino acids 140-421) were expressed as N-terminal glutathione S-transferase (GST) fusion proteins. These fusion proteins were expressed in an *Escherichia coli* CodonPlusRIL (DE3) (Novagene) and purified using a glutathione agarose affinity resin (Peptron, Daejeon, Korea). The GST-tag was cleaved off by treating with thrombin (Invitrogen). In the case of Syn1A and Syb2, 1 g per 100 ml N-octyl- $\beta$ -D-glucopyranoside (OG) was supplemented to maintain these transmembrane proteins in solution. His6-tagged full-length Syt1 was expressed in an *Escherichia coli* BL21 Rosetta (DE3) pLysS (Novagen) and purified using Ni-NTA column. After removing imidazole with PD10 desalting column (GE Healthcare), the eluted Syt1 was kept in the buffer containing 1 g per 100 ml OG.

For the recombinant full-length Syt1 and soluble C2AB, sequence analysis was carried out using T7 promoter/terminator universal primer (COSMO, South Korea), and the existence of glycine at position 374 was confirmed for both proteins. Also, to remove possible nucleic acid contaminants from Syt1 and soluble C2AB, the Syt1-bound Ni-NTA column and the soluble C2AB-bound column were washed two times with the column buffer containing 20 mM  $\text{Ca}^{2+}$  (SI). All these purified proteins were analyzed by 12% SDS-PAGE.

**Reconstitution of membrane proteins into vesicles** The lipid molecules used in this study are 1,2-dioleoyl-sn-glycero-3-phospho-L-serine (DOPS), 1-palmitoyl-2-oleoyl-sn-glycero-3-phosphocholine (POPC), 1,2-dioleoyl-snglycero- 3-phosphoethanolamine (DOPE), phosphatidylinositol-4,5-bisphosphate (PIP<sub>2</sub>, from porcine brain), cholesterol, 1,2-dipalmitoyl-sn-glycero-3-phosphoethanolamin-N-(biotinyl) (biotin-DPPE), 1,1'-dioctadecyl-3,3,3',3'-tetramethylindocarbocyanine perchlorate (DiI, Invitrogen) and 1,1'-dioctadecyl-3,3,3',3'-tetramethylindodicarbocyanine perchlorate (DiD, Invitrogen). All lipids except DiI and DiD were obtained from Avanti Polar Lipids. The molar ratios of lipid species for the full-length Syt1 reactions were 15:31.5:25:20:6:2.5 (DOPS:POPC:DOPE:cholesterol:PIP<sub>2</sub>:DiI) for the t-vesicle, and 3:43.4:25:20:0:0.1:2 (DOPS:POPC:DOPE:cholesterol:PIP<sub>2</sub>:biotin-DPPE:DiD) for the v-vesicle, respectively. Thus, the DOPS concentrations in the v- and t-vesicle membranes were 3 and 15 mol%, respectively and 6 mol% of PIP<sub>2</sub> (S2) was also included for the t-vesicle. However, for the SNARE-only reactions, the DOPS concentration in the v-vesicle membrane was raised to 15 mol% to derive any possible Ca<sup>2+</sup> responsiveness. When the DOPS and the PIP<sub>2</sub> concentrations needed to be changed, the molar ratio of POPC was varied correspondingly to make up the difference.

To reconstitute membrane proteins into vesicles, we first mixed membrane proteins and lipids in the presence of an excess amount of detergent, and then quickly decreased the detergent concentration to below the critical micellar concentration (S3). Driven by the entropy, detergents were squeezed out from lipid-protein-detergent complexes, giving vesicles embedded with membrane proteins as the final product (fig. S1). Specifically,

the lipid mixture was first completely dried and then hydrated by fusion buffer (25 mM HEPES, 0.1 M KCl, 5% glycerol, pH 7.4) containing 1 g per 100 ml OG. The membrane proteins to be reconstituted were dissolved in the same fusion buffer with OG, but in a separate tube. Then, the membrane proteins and the hydrated lipid film were mixed together with the desired lipid to protein ratio. For the fusion reactions with full-length Syt1, we used a ratio of 200:1 for each type of protein (100:1 for SNAP-25), and an increased ratio of 100:1 was used for the SNARE-only reactions (50:1 for SNAP-25). In this final mixture, the lipid concentration should be larger than 1 mM, otherwise aberrant effects by residual detergents would become appreciable. After incubation for 1 hour at 4°C, the lipid-detergent-protein mixture was rapidly diluted by more than three times, bringing the OG concentration to below the critical micelle concentration. This diluted mixture was then dialyzed in 1 L fusion buffer at 4°C for more than 10 hours, with 2 g SM-2 Biobead (Bio-Rad) dissolved in the dialysis buffer. After dialysis, the proteoliposome solution was centrifuged at 10,000 g for 30 min at 4°C and the supernatant was used for the experiment.

For the v-vesicle, Syb2 and Syt1 were first mixed with hydrated lipid films and then mixed together. It is likely that this sequential mixing reduces aggregation of v-vesicles. For the t-vesicle, t-SNARE precomplexes were induced by gently mixing syntaxin 1A and SNAP-25 (1:2 (mol/mol) syntaxin 1A:SNAP-25) at 4°C for 1 hours. This step was done prior to the mixing with the hydrated lipid film. The excess amount of SNAP-25 was used to avoid the complication arising from the inactive precomplex of t-SNAREs (S4). All these mixing steps were done in the presence of 1 g per 100 ml OG.

The vesicle-incorporation rates of proteins were assessed by a coflotation assay (S5). The t-vesicle (or v-vesicle) solution of 400  $\mu$ l was mixed with 400  $\mu$ l 80% Histodenz (Sigma-Aldrich) in a ultracentrifuge tube, and overlaid with 300  $\mu$ l of 30% Histodenz followed by 100  $\mu$ l of fusion buffer. Fusion buffer was used to dissolve the vesicles and Histodenz. Samples were then centrifuged in a SW50 Ti rotor (Beckman) for 2.5 hours at 280,000 g. The vesicles were collected from the 0/30 % Histodenz interface in 350  $\mu$ l, and then concentrated by Ultracel-3K membrane (Millipore) down to 80  $\mu$ l. 40  $\mu$ l sample was analyzed by 15% SDS-PAGE, and the Commassie Blue stained-gel was imaged using Multi Gauge (Fuji film). All the incorporation rates were larger than 25% (fig. S5). We also note that in our single-vesicle assay, un-incorporated proteins, in particular Syt1, could not take part in the fusion reaction. After the immobilization step of the v-vesicles, all the residual vesicles and un-incorporated proteins were completely removed from the microfluidic chamber through microfluidic buffer wash, before the t-vesicle and  $\text{Ca}^{2+}$  ions were introduced for the main reaction.

**Single-vesicle fusion FRET assay** Details of the single-vesicle fusion FRET assay have been described elsewhere (S6, S7). A quartz slide was cleaned using the piranha solution followed by 1 M potassium hydroxide, and then coated with 99:1 (mol/mol) mPEG:biotin-PEG (Laysan Bio). This PEG-treated quartz slide was placed as the bottom surface of a microfluidic chamber (S8) to be used as the imaging surface of our prism-type total internal reflection fluorescence (TIRF) microscopy (based on IX-71, Olympus). To monitor interactions between single v- and t-vesicles, the v-vesicles were attached on

this quartz imaging surface via neutravidin (Invitrogen) that acts as a molecular glue between biotin-PEG and biotinylated lipids (fig. S1). Uniform surface passivation is critical for the success of experiments otherwise the hydrophilic tension of the quartz surface would strongly attract and rupture v-vesicles to form a supported membrane. The t-vesicles (1 to 4  $\mu\text{M}$  [lipids]) and the  $\text{Ca}^{2+}$  ion solution were separately preheated at 37 °C for 10 min and mixed together just prior to the main reaction. We used only deionized water to make the  $\text{Ca}^{2+}$  ion solutions, which seemed to minimize errors in obtaining the prescribed  $\text{Ca}^{2+}$  concentration. This t-vesicle- $\text{Ca}^{2+}$  mixture was introduced into the flow chamber for the fusion reaction, and the temperature was maintained at 37 °C during the reaction.

In the docking-number analysis, we used a computer algorithm that detects local Gaussian maxima in the TIRF images that were recorded by an electron-multiplying charge-coupled device (iXon DU897v, Andor technology) to count the number of the single-vesicle complexes in a given area (Fig. 1A, lower panel)(programs available at <http://bio.physics.illinois.edu/>). Our TIRF microscopy monitored the imaging area of  $45 \times 90 \mu\text{m}^2$  at a time, and we payed particular attention to regulating the number of surface v-vesicles to a uniform level of  $733 \pm 36$  (fig. S3). Therefore, the number of single-vesicle complexes in one imaging area could be directly compared for different molecular conditions (Fig. 1B).

For the real-time tracking measurement, we took movies from fixed imaging areas (also of  $45 \times 90 \mu\text{m}^2$ ) with the time resolution of 100 msec. The imaging buffer including trolox

and the oxygen-scavenging system was used to reduce the photobleaching of dyes. Using the same algorithm as used for the docking-number analysis, each vesicle-vesicle docking event and the subsequent fusion process were individually identified and tracked from the movie (see movie S1). We quantified the FRET efficiency using the equation,  $I_A/(I_D+ I_A)$  where  $I_D$  and  $I_A$  are the donor and acceptor fluorescence intensities respectively. For quantitative analysis of the fusion kinetics, stepwise increases contained in the FRET-efficiency changes were identified by a custom-written MATLAB (Mathwok) program that uses the Schwarz information criterion (*S9*) (Fig. 2, A to D, orange trace)(written by Woori Bae at KAIST).

## Supporting Online Material Text

**SOM Text 1. Analyzing real-time traces** To quantitatively analyze the real-time fusion traces, we adopted a step-finding algorithm that did not require a priori knowledge of the data (S9). A sudden increase of donor fluorescence was taken as the moment of docking, and the moment of full fusion was marked when the FRET efficiency of the single-vesicle complex passes through 0.6 (Fig. 2, A to D and fig. S6). The time gap between these two marks,  $\Delta T$ , was considered the time span required to finish the individual fusion event, thereby exclusively measuring the full fusion kinetics separated from the docking kinetics.

We found that addition of 10  $\mu\text{M}$   $\text{Ca}^{2+}$  to the fusion reaction with membrane-anchored Syt1 considerably accelerated both the docking and the full-fusion kinetics. As a result, in our one-minute movies, we usually saw multiple docking of t-vesicles (for example, fig. S6, A to D). Thus, we classified a real-time trace as a full-fusion event only when the first docking event reached the full fusion state before the second docking occurs as in fig. S6, A and B. When the second docking event seemed to progress to the full-fusion state, we did not consider such real-time trace as a full-fusion event (fig. S6, C and D).

In addition, in many full-fusion events, the transition to the high-FRET state occurred much faster than our time resolution (100 ms) that the real-time trace just appeared as a sudden increase in the acceptor signal without an appreciable change in the donor signal (fig. S6, G and H). In those cases, we set  $\Delta T$  to be 100 ms, which was the time resolution of our measurement. We however expect the actual fusion progression could be faster

than 100 ms, indicating that our measured kinetic rate for full fusion, which is around 400 ms (Fig. 2F), might be an underestimated value.

With these criteria for the full fusion event and  $\Delta T$  measurement, the total docking numbers in our real-time tracking (Fig. 2E) were almost doubled by addition of 10  $\mu\text{M}$   $\text{Ca}^{2+}$  (from 1,166 to 2,234), consistent with the docking-number analysis of Fig. 1B. The probability that such a docking event reaches the full fusion state also increased from 4 to 10 %, which is given by  $(A_1+A_2)/(\text{total docking})$  where  $A_1$  and  $A_2$  are the populations of the fast- and the slow-kinetic components, respectively, found by two-exponential fitting of Fig. 2F. Given such a full fusion event, the probability of obtaining the fast-kinetic component,  $A_1/(A_1+A_2)$ , increased by three times from 21 % to 66 %. These results are summarized in Fig. 2G.

**SOM Text 2. Fluorescence intensity analysis of single-vesicle complexes** It is possible that our in vitro analysis on vesicle docking has been misled by undesired aggregation of vesicles caused by Syt1 and  $\text{Ca}^{2+}$  or by small vesicles with high curvature. To examine this possibility, we placed all the single-vesicle complexes on the graph plane of (FRET efficiency,  $I_A-I_D$ ) and made density plots (fig. S4, left four panels), where  $I_A$  and  $I_D$  were the fluorescence intensities read from the donor and acceptor channels, respectively. The value,  $I_A-I_D$  is expected to increase as the FRET efficiency increases. We collect the single-vesicle complexes placed between two borders of  $0.49(I_A-I_D)_{\text{max}}$  and  $1.69(I_A-I_D)_{\text{max}}$  (rough estimates for 30% difference in size, while and yellow lines in the density plots, respectively), where  $(I_A-I_D)_{\text{max}}$  is the intensity level showing the highest population for a

given FRET efficiency. More than 70% of the total single-vesicle complexes were placed between these two lines for every measurement (fig. S4, rightmost panels). These data tell us that the fusion stimulation by Syt1 predominantly occurs between the single vesicles that are described in fig. S2.

### **SOM Text 3. Modified MWC model for $\text{Ca}^{2+}$ -dependent, non-monotonic activity of**

**Syt1** Our single-vesicle data dissected Syt1's interactions with various partners as illustrated in Fig. 4A. To model the Syt1 activity, we take the following steps.

- i) Our single-vesicle data illustrate that Syt1 must work with both t-SNARE precomplex and  $\text{PIP}_2$  on the trans-membrane for its stimulatory effect (Fig. 4A). Syt1 interacts with the t-SNARE precomplex to catalyze formation of the ternary SNARE complexes. This is best shown by negation of Syt1's stimulation by the sVAMP treatment, which depletes available t-SNARE precomplexes in the reaction. This strict requirement for the t-SNARE precomplex persists even when the cis-membrane interaction is largely weakened (Fig. 4A, black bar and sVAMP treatment).  $\text{PIP}_2$  on the t-vesicle membrane is also essential because decreasing  $\text{PIP}_2$  from 6 to 0.5 mol% also abolishes the stimulation effect (Fig. 4A, blue bar), despite the presence of the t-SNARE precomplex. On the basis of these data, we presume a trans-conformer of Syt1 that can interact with the t-SNARE precomplex and  $\text{PIP}_2$ , and assume that the trans-conformer is required to stimulate fusion.
- ii) We can then naturally assume the other conformer of Syt1, the cis-conformer, which mainly interacts with molecules of its residing membrane, such as PS lipids. When we

remove the PS lipids from the v-vesicle membrane and weaken the cis-membrane interaction, the deactivation pattern selectively vanishes while the stimulatory effect remains largely intact (Fig. 4A, black bar). Therefore, we assume that the cis-conformer is the main cause for Syt1 deactivation.

iii) It has been shown that the trans-membrane interactions with t-SNARE and PIP<sub>2</sub> are fortified with increasing numbers of Ca<sup>2+</sup> bound to Syt1. To take into account, as the first-order approximation, we assume that the degree of fusion stimulation is proportional to the number of Ca<sup>2+</sup> ions bound to Syt1. Certainly, introduction of non-linearity will improve the accuracy of our model, but the main finding of our model, the very different Ca<sup>2+</sup> dissociation constants of the cis- and trans-conformers will stay the same (see below).

We note the cis- and trans-conformers of membrane-anchored Syt1 are analogous to the R and T states in the MWC model. We simply need to adapt the MWC model to include the effect of membrane fusion stimulation.

(a) Syt1 can be either in trans- or in cis-conformer. In analogy to the MWC model, we define the parameters  $L = T_0/C_0$  and  $c = K_{cis}/K_{trans}$ , where  $L$  is the population ratio between trans- and cis-form of Syt1 at zero Ca<sup>2+</sup> concentration and  $K_{cis}$  and  $K_{trans}$  are the dissociation constants for Ca<sup>2+</sup>-binding. Because Syt1 can bind to up to five Ca<sup>2+</sup> ions, the probability that one finds membrane-anchored Syt1 in the trans-conformer with  $i$  Ca<sup>2+</sup>

ions bound is given as:  $P_{trans}(i) = \frac{{}_5C_i L (c\alpha)^i}{(1 + \alpha)^5 + L(1 + c\alpha)^5}$ , where  $\alpha = [Ca^{2+}] / K_{cis}$ .

(b) Even if the trans-conformer has been promoted by  $\text{Ca}^{2+}$  ions, interaction with the t-SNARE precomplex is absolutely required for the trans-conformer to finally stimulate fusion. If we neglect cooperativity in the interaction between the Syt1 and t-SNARE precomplex (i.e., simply one-to-one reaction), we can introduce a reactivity function,  $\kappa_t$ , which has a constant value of unity when there is a t-SNARE precomplex available to interact with Syt1.  $\kappa_t$  becomes zero when t-SNARE precomplex is not available. Then, the final form of  $P_{\text{trans}}(i)$  is given as:

$$P_{\text{trans}}(i) = \kappa_t \frac{{}_5C_i L(c\alpha)^i}{(1 + \alpha)^5 + L(1 + c\alpha)^5}, \quad (\text{Eq. 1}).$$

(c) As assumed above, the degree of fusion stimulation is proportional to the number of  $\text{Ca}^{2+}$  ions bound to the trans-form of Syt1. Thus, the dynamic activity of Syt1 is

$$\text{proportional to } \sum_i iP_{\text{trans}}(i) = \sum_i \kappa_t \frac{i {}_5C_i L(c\alpha)^i}{(1 + \alpha)^5 + L(1 + c\alpha)^5} = \kappa_t \frac{5Lc\alpha(1 + c\alpha)^4}{(1 + \alpha)^5 + L(1 + c\alpha)^5}.$$

We finally add two baseline properties  $S_{\text{no\_Ca}^{2+}}$  and  $S_{\text{sVAMP}}$  to account for the Syt1 activity at  $0 \mu\text{M Ca}^{2+}$  and that obtained without t-SNARE precomplex (the sVAMP data), respectively.

From (a) to (c), the population of single-vesicle complexes at a given  $\text{Ca}^{2+}$  concentration is:

$$N(\alpha) = N_0 \left[ \kappa_t \left\{ \frac{5Lc\alpha(1 + c\alpha)^4}{(1 + \alpha)^5 + L(1 + c\alpha)^5} + S_{\text{no\_Ca}^{2+}} \right\} + S_{\text{sVAMP}} \right], \quad (\text{Eq. 2})$$

where  $N_0$  is the total number of surface-immobilized v-vesicle (assumed to be 1,000 here).

$S_{sVAMP}$  was determined to give  $N_0 S_{sVAMP}$  the number of single-vesicle complexes observed when treated with sVAMP, and then  $S_{no\_Ca^{2+}}$  was determined to give  $N_0(S_{no\_Ca^{2+}} + S_{sVAMP})$  the number of single-vesicle complexes obtained at 0  $\mu\text{M}$   $\text{Ca}^{2+}$ . We note that Eq.2 is a non-monotonic function of  $[\text{Ca}^{2+}]$  for a certain range of parameter set.

The fitting using this model with five ligand binding sites ( $n=5$ , fig. S7, solid line) was in excellent agreement with the single-vesicle docking data, enabling us to extract the  $\text{Ca}^{2+}$  dissociation constants ( $K_{cis}$  and  $K_{trans}$ ) of the cis- and trans-conformers. In addition, this result could be generalized to include  $n$  different from five, where then  $n$  plays a role of the general Hill coefficient (fig. S7, dashed line fitting). With  $L=400$  (see the discussion below), the PS-3 mol% data were fit with the parameters  $n=5$  (fixed),  $c=K_{cis}/K_{trans}=0.029$ ,  $K_{cis}=5.4 \mu\text{M}$  (i.e,  $K_{trans}=186.2 \mu\text{M}$ )(fig. S7, red solid curve) or with the parameters  $n=6.5$ ,  $c=K_{cis}/K_{trans}=0.037$ ,  $K_{cis}=8.7 \mu\text{M}$  (i.e,  $K_{trans}=235.13 \mu\text{M}$ )(red dashed curve). The PS-15 mol% data with 1 mM  $\text{Mg}^{2+}$  were fit with the parameters  $n=5$  (fixed),  $c=K_{cis}/K_{trans}=0.015$ ,  $K_{cis}=4.7 \mu\text{M}$  (i.e,  $K_{trans}=313.3 \mu\text{M}$ )(black solid curve) or with the parameters  $n=3.1$ ,  $c=K_{cis}/K_{trans}=0.012$ ,  $K_{cis}=1.4 \mu\text{M}$  (i.e,  $K_{trans}=116.66 \mu\text{M}$ )(black dashed curve).

It is noteworthy that the condition of  $L \gg 1$  and  $c \ll 1$  is required to have a best fit to the single-vesicle data, which is identical to the condition for the cooperative oxygen uptake behavior in the original MWC model. For  $c=1$ , Eq. 2 is simplified to

$$N(\alpha) = N_0 \left[ \kappa_t \left\{ \frac{nL\alpha}{(1+L)(1+\alpha)} + S_{no\_Ca^{2+}} \right\} + S_{sVAMP} \right] \approx N_0 \left[ \kappa_t \frac{n\alpha}{(1+\alpha)} + O(0.1) \right], \text{ which is}$$

however a monotonically increasing function of  $\alpha$ .

**Estimation of the  $L$  value** :  $L$  is effectively an equilibrium constant between the cis- and trans-conformers in the absence of  $\text{Ca}^{2+}$ ;  $L = T_0/C_0$ . To estimate  $L$  value, we separately consider changes in enthalpy and entropy associated with the  $C_0 \rightarrow T_0$  process.

(i) The energetic contribution of the  $C_0$  form comes from the contact energy of  $\text{Ca}^{2+}$ -binding loop to the *cis*-membrane. The  $\text{Ca}^{2+}$ -binding loops in Syt1 have in assumed to have four negatively-charged residues in total at the binding interface with the membrane. Since membranes are also negatively charged, the interaction energy between the C2AB loop and *cis*-membrane is mostly determined by the electrostatic repulsion in the absence of  $\text{Ca}^{2+}$  ion that can mediate the loop-membrane interactions. We estimate the enthalpic (energetic) contribution to be:

$$\Delta E_{C_0 \rightarrow T_0} \sim (0 - 4 \times \frac{l_B}{r}) e^{-\kappa_D r} \times k_B T \approx -4.7 k_B T \quad (\text{Eq. 3}),$$

where  $l_B \approx 7 \text{ \AA}$  is the Bjerrum length,  $\kappa_D = \sqrt{8\pi l_B c} \approx 0.1 \text{ \AA}^{-1}$  is the inverse Debye screening length under 100 mM monovalent salt condition, and  $r \approx 4 \text{ \AA}$  at the contact distance.

(ii) The entropic contribution due to the conformational change of Syt1 from  $C_0$  to  $T_0$  form can be estimated by calculating the volume accessible by each form,  $V_{C_0}$  and  $V_{T_0}$ . Syt1 is made of 418 residues that includes the C2A (residue 140-261) and C2B domain (residue 275-418). The radius of gyration for C2A and C2B is  $R_G^{C2A} \approx R_G^{C2B} \approx 3 \text{ nm}$ , and the size of the linker part between the transmembrane domain and C2AB (about 60 residues, residue 70-139) can be estimated using Flory law as  $R_l \sim a N^{3/5} \sim (3.8 \text{ \AA})(60)^{3/5} \approx 4$

nm. Hence, the volume explored by the trans conformer of Syt1 is estimated as

$V_{T_0} \sim (2/3)\pi d^3$  where  $d = 2 \times (R_0 + R_G^{C2A} + R_G^{C2B})$ . Meanwhile, the disk shape volume

explored by the cis-form of Syt1 is  $V_{C_0} \sim \pi d^2 R_0$ . Therefore, the entropic contribution of

$C_0$  to  $T_0$  form is:

$$-T\Delta S_{C_0 \rightarrow T_0} = -k_B T \log\left[\frac{V_{T_0}}{V_{C_0}}\right] \approx -k_B T \log\left[\frac{2d}{3R_0}\right] \approx -1.2k_B T, \quad (\text{Eq. 4}).$$

Finally, from (i) and (ii) our *rough* estimate of total free energy change associated with

$C_0 \rightarrow T_0$  process is  $\Delta F (= \Delta E - T\Delta S) \approx -6k_B T$ , leading to  $L = e^6 \approx 400$ .

#### **SOM Text 4. Effects of soluble C2AB on SNARE-mediated membrane fusion**

**studied by the single-vesicle fusion assay** The transmembrane domain-truncated Syt1

variant, soluble C2AB, was mixed with the t-vesicle and injected onto the surface-

immobilized, SNARE-only v-vesicles. As in other SNARE-only reactions, the PS lipids

of the v-vesicle membrane was 15 mol% and 1 mM  $\text{Mg}^{2+}$  ions were included in the

fusion buffer. After a three-second reaction, aqueous buffer containing the preset  $\text{Ca}^{2+}$

concentration (as well as 1 mM  $\text{Mg}^{2+}$ ) was introduced to remove floating vesicles and

proteins. We used 4 nM for the soluble C2AB because this is the concentration

equivalent to that of the membrane-anchored Syt1 used in this work;  $4 \text{ nM} = 4 \mu\text{M}$

$[\text{lipid}] \times (1/200) \times 1/2.5 \times 1/2 = \text{vesicle conc.} [\text{lipid}] \times \text{protein-lipid ratio} \times \text{vesicle-}$

incorporation rate  $\times$  bilayer factor. At this same effective concentration, the soluble

C2AB stimulated the single vesicle-vesicle docking in response to  $100 \mu\text{M} \text{Ca}^{2+}$  (Fig. 4D

and fig. S9), requiring one order of magnitude higher  $\text{Ca}^{2+}$  than the membrane-anchored

Syt1. Protein-DNA interactions and scaffolding proteins take advantage of reduced dimensionality or localization effects to enhance consequent biochemical reactions. Confining Syt1's movements within a two-dimensional surface of 50 nm vesicles may greatly reduce the entropic cost for the search dynamics, allowing Syt1 to more effectively interact with the t-SNAREs and anionic lipids than the soluble C2AB that freely diffuses and rotates in a three-dimensional space of aqueous buffer.

It is also noteworthy that this docking simulation by soluble C2AB does not show a propensity for deactivation up to 500  $\mu\text{M}$   $\text{Ca}^{2+}$  (Fig. 4D and fig. S9). What is the principal difference between the soluble C2AB and membrane-anchored Syt1? There should be a wide variability in the orientation of C2AB binding at the fusion site, but the conformational entropy of Syt1 could be largely restricted by membrane anchoring to the vesicular membrane (Fig. 4E). For example, the C2B domain becomes proximal more likely to the trans-membrane than to the cis-membrane. Such a restricted conformation of Syt1 may be essential for the 'tug-of-war' between the cis- and trans-conformers, and consequently for the  $\text{Ca}^{2+}$ -dependent, non-monotonic activity of Syt1.

## Supplementary Figures

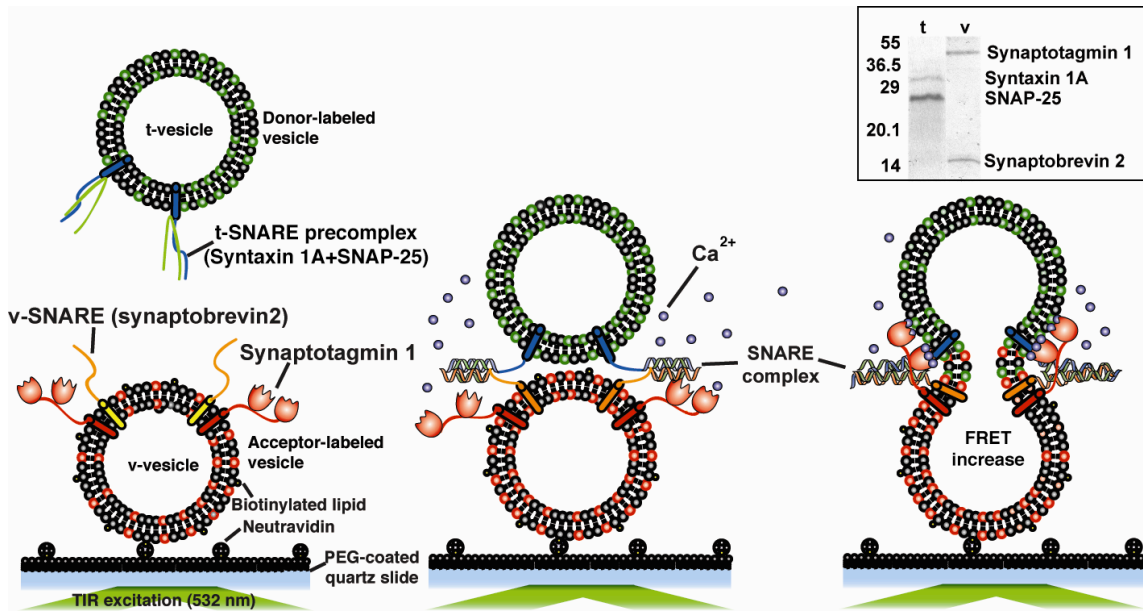


**fig. S1. Schematic of the single-vesicle fusion FRET assay.** (Inset), protein composition of the t- and v-vesicles assessed by SDS-PAGE and Coomassie staining.

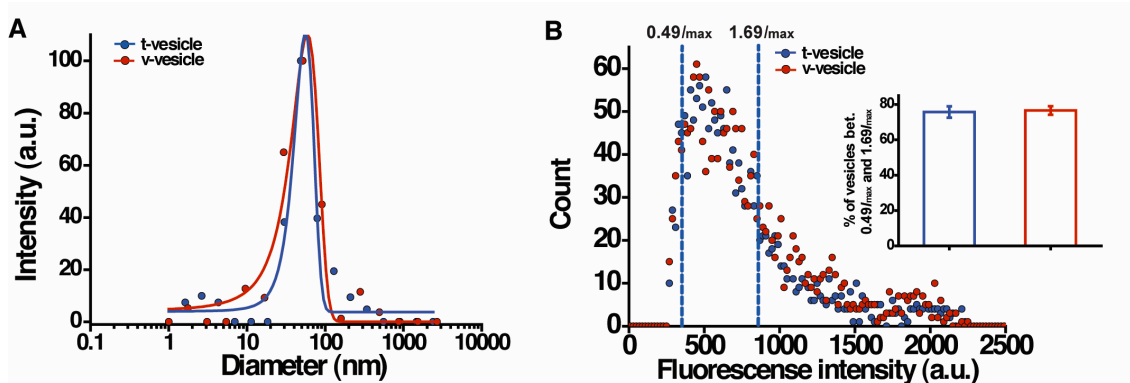


**fig. S2. Physical size of t- and v-vesicles.** (A) Dynamic light scattering measurement showed that both t- (blue) and v-vesicles (red) have a Gaussian distribution in the hydrodynamic diameter, with peak at 50 nm and the standard deviations around 20 nm. (B) Left, fluorescence intensity distributions of the t- (blue symbols) and v-SNARE vesicles (red). For single-vesicle fluorescence imaging, both vesicles were labeled with 2 mol% DiI. Right, the percentage of single-vesicle complexes included in the range between  $0.49I_{\max}$  and  $1.69I_{\max}$  ( $I_{\max}$  is the fluorescence intensity with the highest population), which corresponds to 30% difference in the size. 75.7 % and 76.6 % of the t- and the v-SNARE vesicles belong in the specified range respectively. All errors are SD unless otherwise specified.

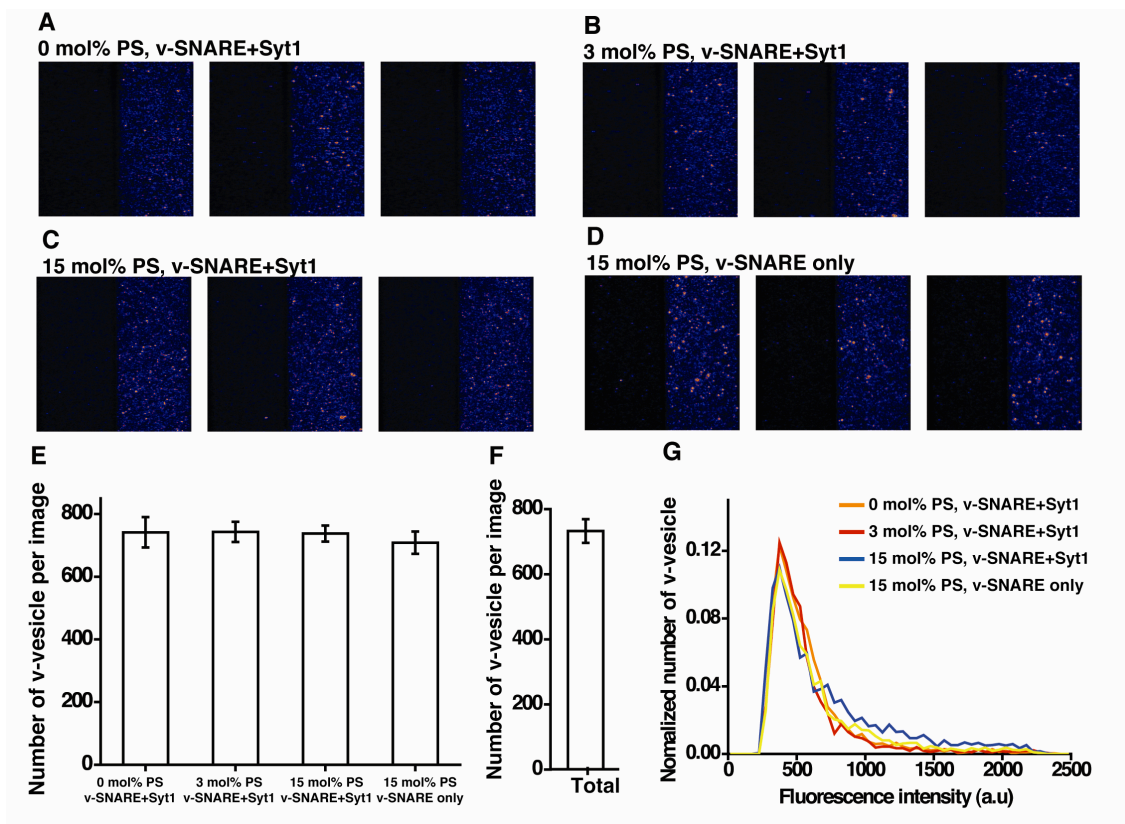
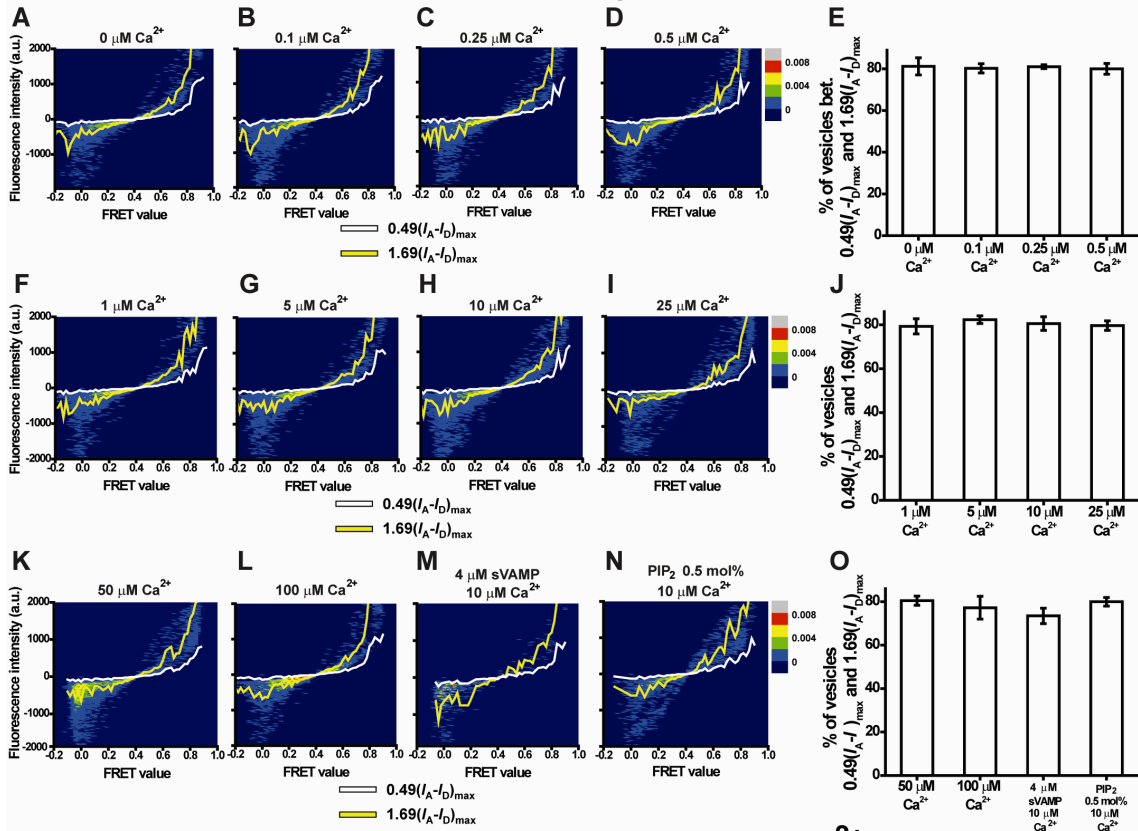
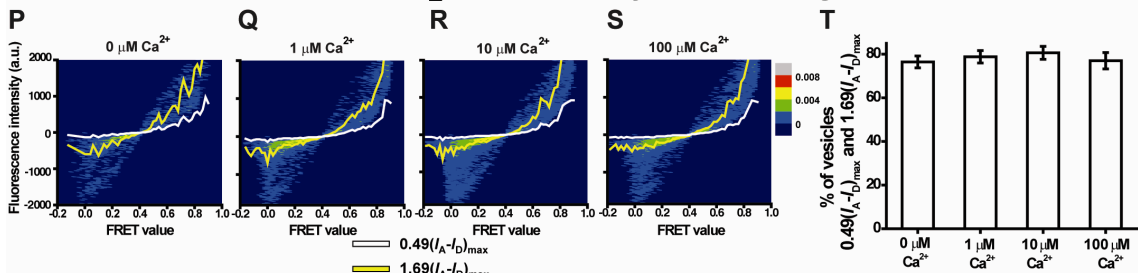


**fig. S3. Population of surface-immobilized v-vesicles per imaging area. (A-D)** Exemplary TIRF snapshots of the v-vesicle coverage for different lipid and protein compositions used in this work. **(E and F)** Count of surface-immobilized v-vesicles per imaging area. Despite different molecular conditions for v-vesicles, the numbers of surface-immobilized v-vesicles in one imaging area ( $45 \times 90 \mu\text{m}^2$ ) showed a constant level **(E)**. Even when all the cases were pooled together, the number of v-vesicles per imaging area showed a narrow distribution of  $733 \pm 36$  **(F)**. **(G)** Fluorescence intensity distributions of the individual v-vesicles. The similarity between the distributions indicates that all the types of v-vesicles with different PS and protein compositions should have a similar size distribution as shown in fig. S2. All errors are SD unless otherwise specified.

v: 3 mol% PS, t: 6 mol% PIP<sub>2</sub> , [SNARE+Syt1]



v: 15 mol% PS, t: 6 mol% PIP<sub>2</sub> , [SNARE+Syt1], 1 mM Mg<sup>2+</sup>



v: 15 mol% PS, t: 6 mol% PIP<sub>2</sub> , [SNARE], 4 nM C2AB+1 mM Mg<sup>2+</sup>

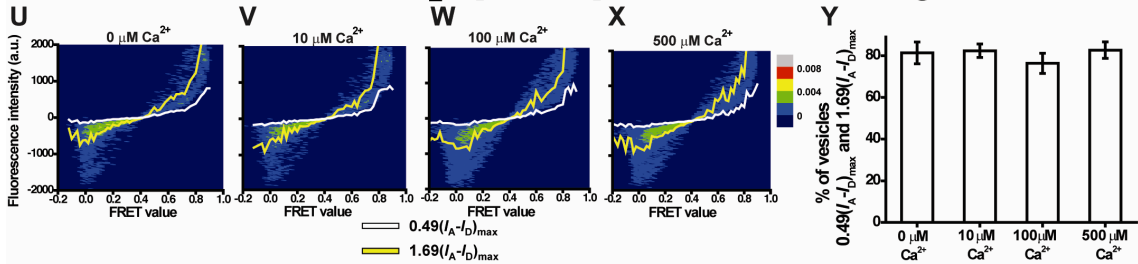
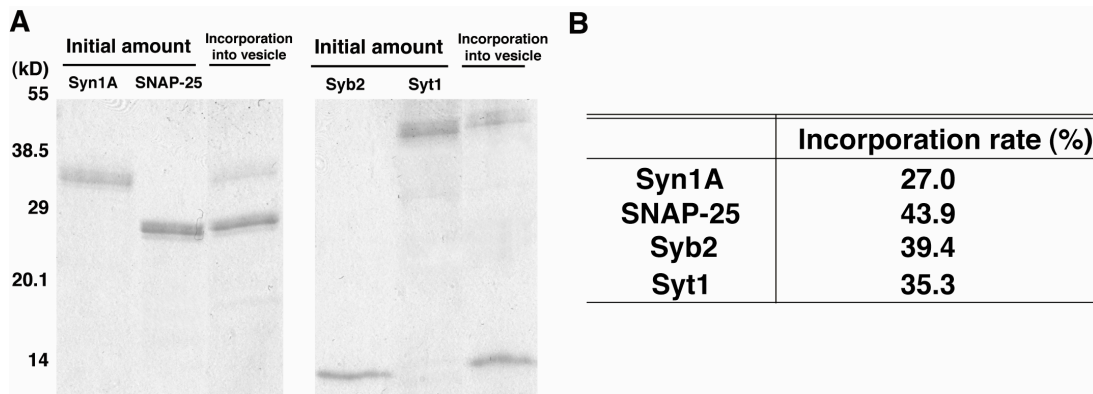


fig. S4. Fluorescence-intensity analysis of single-vesicle complexes. (Left four panels)

Fluorescence intensity analyses of single-vesicle complexes under the molecular

conditions depicted (see SOM Text 2). 15 mol% PS was included for the t-vesicle in every case. **(Rightmost panels)** Percentage of single-vesicle complexes placed between  $0.49(I_A-I_D)_{\max}$  and  $1.69(I_A-I_D)_{\max}$  (while and yellow lines), where  $(I_A-I_D)_{\max}$  is the intensity level showing the highest population for a given FRET efficiency. All errors are SD unless otherwise specified.



**fig. S5. Vesicle-incorporation rate of SNAREs and membrane-anchored Syt1.** (A) SDS-PAGE gel results of the cofloatation assay (see Materials and Methods). (B) Vesicle-incorporation rate of the four membrane proteins used in this study.

V: 3 mol% PS, t: 6 mol% PIP<sub>2</sub>

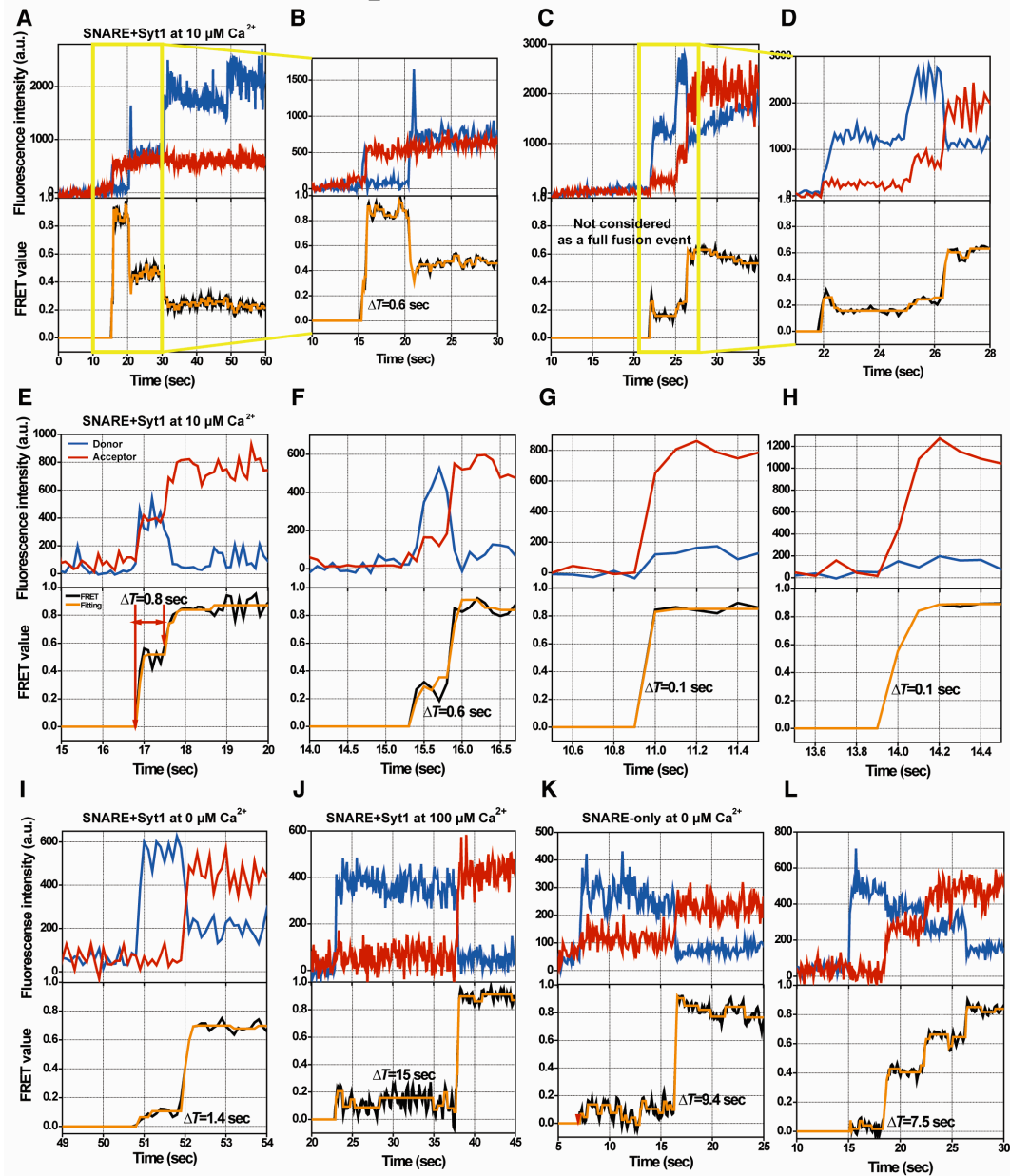


**fig. S6. Real-time traces of single vesicle-vesicle fusion events.** Fusion reactions were induced under the molecular conditions depicted. 15 mol% PS was included for the t-vesicle in every case. Upper panel, the changes in the donor (green) and the acceptor (red) fluorescence intensities. Low panel, the corresponding changes in the FRET (black) and stepwise increases in the FRET signal identified by Schwarz information criterion (orange).

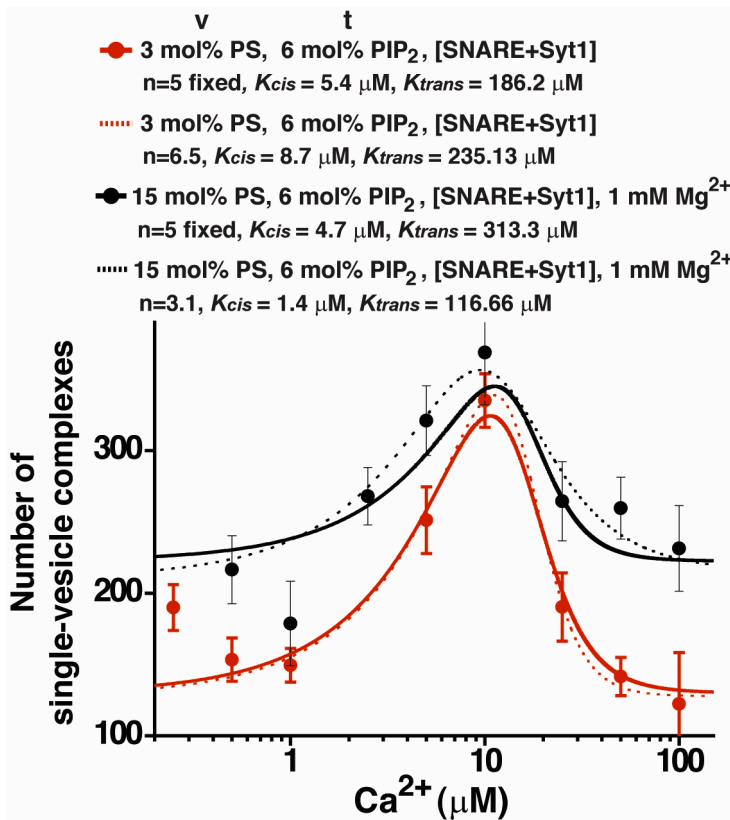


**fig. S7. Modified MWC model fitting of Ca<sup>2+</sup>-dependent, non-monotonic activity of Syt1.** The fitting using the modified MWC model (SOM text 3) with five ligand binding sites ( $n=5$ ; solid lines) is in excellent agreement with the single-vesicle docking data, enabling us to extract the Ca<sup>2+</sup> dissociation constants ( $K_{cis}$  and  $K_{trans}$ ) of the cis- and trans-conformers. In addition, this result can be generalized to include  $n$  different from five, where then  $n$  plays a role of the general Hill coefficient (dashed line fittings). All errors are SD unless otherwise specified.

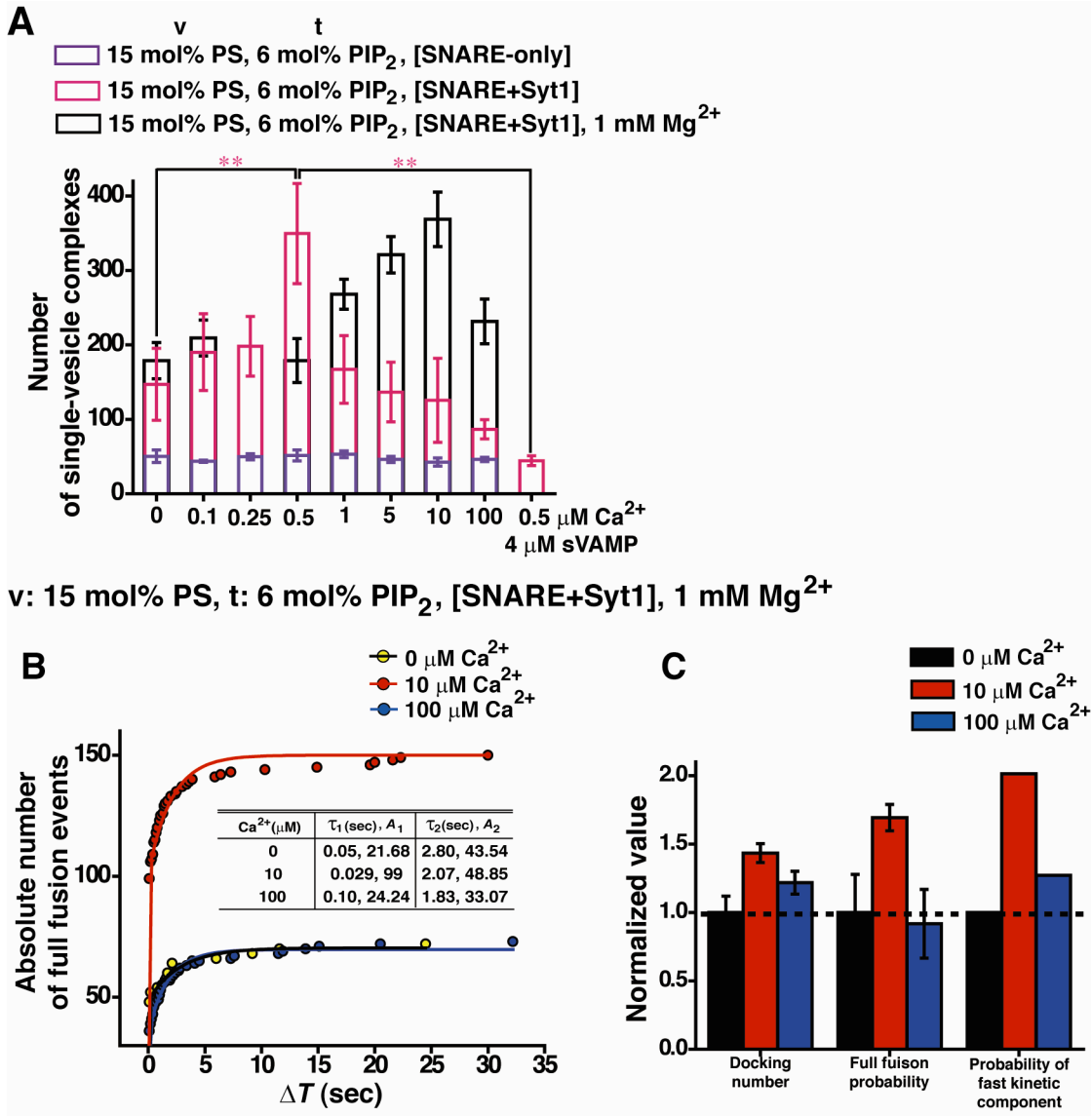


**fig. S8.  $\text{Ca}^{2+}$ -dependent, non-monotonic activity of the membrane-anchored Syt1, observed with physiological PS concentrations in fusing membranes. (A) Single-vesicle docking data obtained with 15 mol% PS lipids in both t- and v-vesicles. (B) Corresponding changes of the full-fusion kinetics studied by the real-time tracking approach. The analysis methods are the same as that of Fig. 2, E and F. (C) Acceleration of different fusion steps as a function of  $\text{Ca}^{2+}$  used. The analysis method is the same as that of Fig. 2G (see also SOM text 1). All errors are SD unless otherwise specified.**

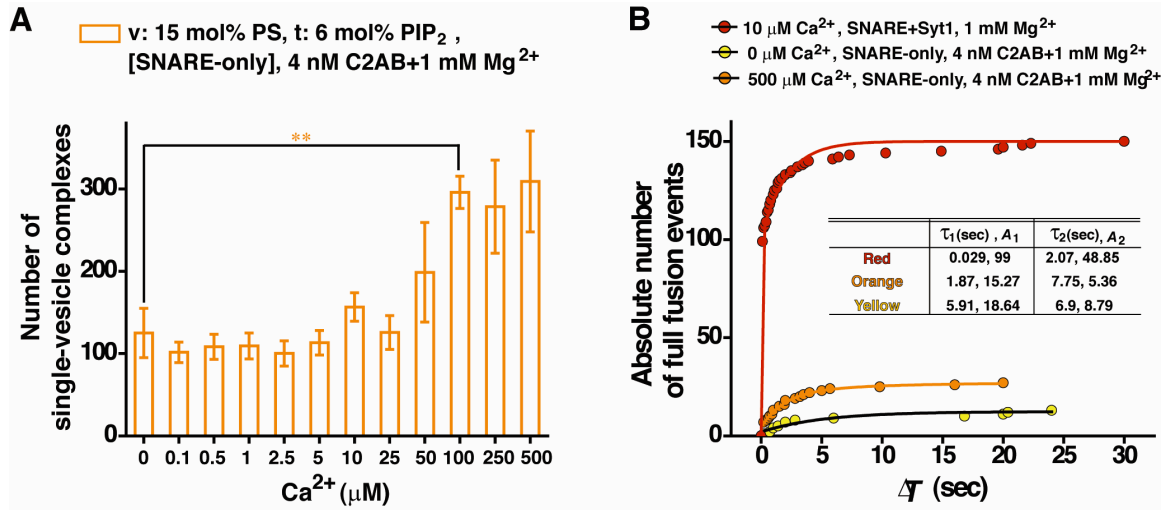


**fig. S9. Effects of soluble C2AB on SNARE-mediated membrane fusion studied by the single-vesicle fusion assay. (A)** Single-vesicle docking stimulated by 4 nM soluble C2AB at different Ca<sup>2+</sup> concentrations. **(B)** Corresponding acceleration of the full fusion kinetics. Cumulative  $\Delta T$  distributions of the full fusion reaction carried out at 0 μM (yellow symbols and curve) and 500 μM Ca<sup>2+</sup> (orange). For comparison, the membrane-anchored Syt1 data under the same reaction conditions are revisited from fig. S8B (red symbols and curve). All errors are SD unless otherwise specified.

**Table S1. Number of single-vesicle complexes studied in this work**

| SNARE+Syt1                           |  |
|--------------------------------------|--|
| Ca <sup>2+</sup> (μM)                | v: 0 mol% PS, t: 6 mol% PIP <sub>2</sub> |
| 0                                    | 3,376                                    |
| 0.1                                  | 6,481                                    |
| 0.25                                 | 7,145                                    |
| 0.5                                  | 6,843                                    |
| 1                                    | 7,600                                    |
| 5                                    | 7,430                                    |
| 10                                   | 6,991                                    |
| 100                                  | 6,591                                    |
| 0.5 μM Ca <sup>2+</sup> , 4 μM sVAMP | 1,967                                    |

| Ca <sup>2+</sup> (μM)                | SNARE-only<br>v: 3 mol% PS,<br>t: 6 mol% PIP <sub>2</sub> | SNARE+Syt1<br>v: 3 mol% PS,<br>t: 6 mol% PIP <sub>2</sub> | SNARE+Syt1<br>v: 3 mol% PS,<br>t: 0.5 mol% PIP <sub>2</sub> |
|--------------------------------------|---|---|---|
| 0                                    | 6,513   | 3,252   | 3,570   |
| 0.1                                  | 6,054   | 4,479   | 4,215   |
| 0.25                                 | 6,231   | 3,799   | 3,744   |
| 0.5                                  | 5,962   | 3,067   | 2,925   |
| 1                                    | 6,153   | 2,986   | 3,060   |
| 5                                    | 5,914   | 5,025   | 4,245   |
| 10                                   | 5,187   | 6,702   | 3,660   |
| 25                                   | 5,770   | 11,410  | -   |
| 50                                   | 6,153   | 8,494   | -   |
| 100                                  | 5,962   | 7,344   | 4,161   |
| 10 μM Ca <sup>2+</sup><br>4 μM sVAMP | 717   | 1,734   |   |

| Ca <sup>2+</sup> (μM) | SNARE-only<br>v: 15 mol% PS,<br>t: 6 mol% PIP <sub>2</sub> | SNARE+Syt1<br>v: 15 mol% PS,<br>t: 6 mol% PIP <sub>2</sub> |
|-----------------------|--|--|
| 0                     | 3,018  | 8,821  |
| 0.1                   | 2,616  | 11,403   |
| 0.25                  | 2,979  | 11,886   |
| 0.5                   | 3,090  | 20,977   |
| 1                     | 3,180  | 10,021   |
| 5                     | 2,760  | 8,187  |
| 10                    | 2,550  | 7,525  |
| 100                   | 2,766  | 5,187  |

| Ca <sup>2+</sup> (μM)               | SNARE-only   | SNARE+Syt1   |
|-------------------------------------|--|--|
|                                     | v: 15 mol% PS,<br>t: 6 mol% PIP <sub>2</sub> ,<br>with 1 mM Mg <sup>2+</sup> | v: 15 mol% PS,<br>t: 6 mol% PIP <sub>2</sub> ,<br>with 1 mM Mg <sup>2+</sup> |
| 0                                   | 3,132  | 7,151  |
| 0.1                                 | 3,248  | 8,370  |
| 0.5                                 | 3,440  | 8,660  |
| 1                                   | 3,166  | 7,152  |
| 2.5                                 | 2,528  | 10,722   |
| 5                                   | 2,514  | 12,840   |
| 10                                  | 2,676  | 14,752   |
| 25                                  | 2,822  | 10,580   |
| 50                                  | 2,394  | 10,386   |
| 100                                 | 2,530  | 9,258  |
| 10 μM Ca <sup>2+</sup> , 4 μM sVAMP | -  | 2,687  |

| Ca <sup>2+</sup> (μM) | SNARE-only  |
|-----------------------|---|
|                       | v: 15 mol% PS, t: 6 mol% PIP <sub>2</sub> ,<br>with 4 nM C2AB + 1 mM Mg <sup>2+</sup> |
| 0                     | 5,002   |
| 0.1                   | 4,062   |
| 0.5                   | 4,328   |
| 1                     | 4,370   |
| 2.5                   | 4,008   |
| 5                     | 4,530   |
| 10                    | 6,264   |
| 25                    | 5,026   |
| 50                    | 7,948   |
| 100                   | 11,832  |
| 250                   | 11,138  |
| 500                   | 12,362  |

## Movie S1

**(Center panel)** Donor and acceptor images of one imaging area directly recorded from the TIRF microscopy. This movie was included in the three real-time movies that were used to make the cumulative  $\Delta T$  plot of Fig. 2E (red symbols). To help viewers see the events, the playing speed is slowed down by six times compared with the real-time speed.

**(Left and right panels)** Four representative, individual single-vesicle fusion events. Enlarged images of the donor- and acceptor-channel signals and the corresponding time traces are shown for each fusion event. Their respective positions in the total imaging area are depicted in the center panel.

## References

- S1. J. Ubach *et al.*, *Biochemistry* **40**, 5854 (2001).
- S2. D. J. James, C. Khodthong, J. A. Kowalchuk, T. F. Martin, *J Cell Biol* **182**, 355 (2008).
- S3. J. L. Rigaud, D. Levy, *Methods Enzymol* **372**, 65 (2003).
- S4. A. V. Pobbati, A. Stein, D. Fasshauer, *Science* **313**, 673 (2006).
- S5. W. C. Tucker, T. Weber, E. R. Chapman, *Science* **304**, 435 (2004).
- S6. T. Y. Yoon, B. Okumus, F. Zhang, Y. K. Shin, T. Ha, *Proc Natl Acad Sci U S A* **103**, 19731 (2006).
- S7. T. Y. Yoon *et al.*, *Nat Struct Mol Biol* **15**, 707 (2008).
- S8. R. Roy, S. Hohng, T. Ha, *Nat Methods* **5**, 507 (2008).
- S9. B. Kalafut, K. Visscher, *Computer Physics Communications* **179**, 716 (2008).